

Article

Micro-Electromechanical Acoustic Resonator Coated with Polyethyleneimine Nanofibers for the Detection of Formaldehyde Vapor

Da Chen ^{1,2,*}, Lei Yang ², Wenhua Yu ², Maozeng Wu ², Wei Wang ² and Hongfei Wang ²

¹ State Key Laboratory of Mining Disaster Prevention and Control Co-founded by Shandong Province and the Ministry of Science and Technology, Shandong University of Science and Technology, Qingdao 266590, China

² College of Electronics, Communications, and Physics, Shandong University of Science and Technology, Qingdao 266590, China; ylei1994@163.com (L.Y.); 17860756595@163.com (W.Y.); wumaozeng1993@163.com (M.W.); skdwangwei1zqf@163.com (W.W.); phywj@163.com (H.W.)

* Correspondence: chenda@sdust.edu.cn; Tel.: +86-0532-8605-7555

Received: 19 December 2017; Accepted: 26 January 2018; Published: 1 February 2018

Abstract: We demonstrate a promising strategy to combine the micro-electromechanical film bulk acoustic resonator and the nanostructured sensitive fibers for the detection of low-concentration formaldehyde vapor. The polyethyleneimine nanofibers were directly deposited on the resonator surface by a simple electrospinning method. The film bulk acoustic resonator working at 4.4 GHz acted as a sensitive mass loading platform and the three-dimensional structure of nanofibers provided a large specific surface area for vapor adsorption and diffusion. The ultra-small mass change induced by the absorption of formaldehyde molecules onto the amine groups in polyethyleneimine was detected by measuring the frequency downshift of the film bulk acoustic resonator. The proposed sensor exhibits a fast, reversible and linear response towards formaldehyde vapor with an excellent selectivity. The gas sensitivity and the detection limit were 1.216 kHz/ppb and 37 ppb, respectively. The study offers a great potential for developing sensitive, fast-response and portable sensors for the detection of indoor air pollutions.

Keywords: film bulk acoustic resonator; formaldehyde; gas sensor; nanofibers

1. Introduction

Formaldehyde, usually derived from household materials, is one of the most common indoor air pollutants. There is a strong demand for a sensitive, fast-response and portable method to detect formaldehyde for indoor environmental monitoring due to its high carcinogenicity [1]. The traditional spectroscopy, chromatography and mass spectrometry are very hypersensitive, accurate and reliable, but they are limited by the large-scale equipment, professional operation and unable to detect formaldehyde at a customer's home [2]. The solution leads to the development of smart formaldehyde sensors with small device size and rapid response speed. So far, metal oxide semiconductor (MOS) [3–5], carbon nanotubes (CNTs) [6–8], conductive polymer [9] have been used to fabricate formaldehyde sensors based on field effect, resistive and electroacoustic principles. Over the past decade, the technical progress in micro-electromechanical systems (MEMS) brings a novel development direction for the microsensors.

Film bulk acoustic resonator (FBAR) is a promising microelectromechanical system (MEMS) resonator and has obtained the preliminary success in radio frequency communication technologies [10–12]. Moreover, its applications for gas [13–16] and biochemical detections [17–20] have received attention thanks to the high sensitivity and micron-scale size. Compared with the conventional electroacoustic resonator such as quartz crystal microbalance (QCM), the important advance of FBAR is the use of

1–2 microns-thick piezoelectric films to replace the crystal plates, which provides a fundamental working frequency at several gigahertz and enough mass sensitivity to probe a single gas molecules layer [21,22]. In addition, FBAR is fabricated by standard MEMS process, thereby realizing the ability to inexpensively combine a number of sensors on a chip and integrate them with the analytical circuits. For gas-sensing applications, the FBAR usually works as a mass-loading platform. A sensitive layer is coated on the device surface to absorb the target molecules. The small additional mass on the sensing layer is detected by monitoring the variation of resonant frequency. As a result, the properties of sensitive coating determine the molecule recognitions, and directly affect the sensitivity, stability and reversibility of the sensor. Up to now, a variety of sensitive coatings, such as polymers [23,24], proteins [25–27], aptamers [28–31], enzymes [32,33], supramolecular monolayers [34,35], hydrophilic film [23] and CNTs [36] have been employed for FBAR sensors to achieve the selectivity for different analytes.

Polyethyleneimine (PEI) and its derivatives are regarded as an appropriate formaldehyde-sensitive material since PEI can efficiently adsorb formaldehyde molecules via a reversible reaction of primary amines. Therefore, polystyrene (PS)/PEI [37], poly(vinyl alcohol) (PVA)/PEI [38], TiO₂/PEI [39], and CNTs/PEI composites [40] have been reported as the sensitive coating of mass-loading sensors for the detection of formaldehyde vapor. On the other hand, in the view of the high sensitivity of FBAR devices, the nanostructured materials featured with high surface areas and numerous sites are the potential coating for gas sensing.

In this paper, we developed a promising strategy to combine PEI nanofibers and the FBAR with high mass sensitivity to construct a formaldehyde microsensor. The PEI nanofibers were directly deposited on an AlN FBAR surface by a simple electrospinning method. Benefiting from the high working frequency at 4.4 GHz, the proposed FBAR was able to measure the ultra-small mass change produced by the interaction between formaldehyde molecules and the PEI nanofibers with linear response characteristics, fast response/recovery rate and excellent selectivity.

2. Device Configuration and Fabrication

2.1. Schematic Structure and Sensing Mechanism

Figure 1a,b shows the schematic structure, sensing mechanism and the photomicrograph of the FBAR formaldehyde sensor. The major structure of FBAR ($300 \times 150 \mu\text{m}^2$) is a sandwiched Au (100 nm)/AlN (1 μm)/Mo (100 nm) piezoelectric stack built on a Si₃N₄ sputtered layer (0.6 μm). The PEI nanofibers were deposited on the surface of top Au electrode as the specific sensitive coating. The active resonance and sensing area are overlapped between the two electrodes ($3296 \mu\text{m}^2$). When the FBAR sensor is exposed to gaseous formaldehyde, the reversible nucleophilic addition reaction happens between the amines of PEI and the vapor molecules at room temperature [41]. In fact, there is a σ -bond and a π -bond in the formaldehyde molecule. Because of the difference in electron affinity, the oxygen atom side shows electronegativity while the positive side of carbon atoms can be considered as the electrophile. In the amine group, the lone pair in the nitrogen atoms works as the nucleophile and engages in the reaction with the π -bond in formaldehyde molecules. Therefore, the vapor absorption can be measured by monitoring the downshift of resonant frequency based on the mass-sensitive mechanism.

In order to minimize the environmental disturbance, the practical differential frequency method was used to extract the sensing response as shown in Figure 1c. For this purpose, both the FBAR coated with PEI nanofibers and the reference FBAR device (without coating) were wire-bonded to a printed circular board (PCB) and packaged in the test chamber (Figure 1d). Upon the exposure of formaldehyde, the resonant frequency of the former device decreased while the reference frequency measured from the latter kept stable. The frequency difference between the two devices was read out by a testing circuit as the sensing response to formaldehyde vapor. All components in the test circuit were off-the-shelf. At first, the two FBAR devices were driven by independent Colpitts oscillators.

The frequency signals were put into the mixer and then passed through the balun transformer, low-pass filtered, the amplified, waveform converter and frequency dividing circuits. At last, a micro controller unit was used to count, read out and store the differential frequency. The details of the circuit design were shown in Supplementary Material (Figure S1).

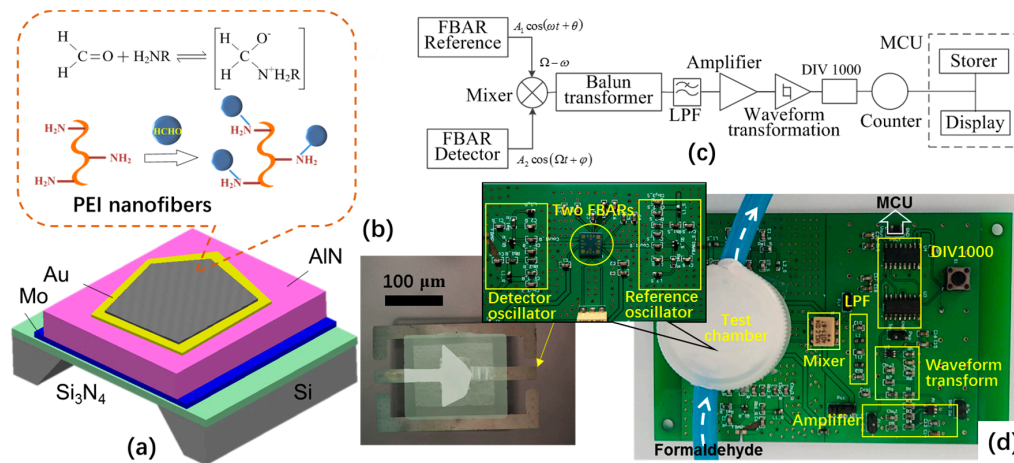


Figure 1. (a) Schematic structure and sensing mechanism of the film bulk acoustic resonator (FBAR) sensor coated with polyethyleneimine (PEI) nanofibers; (b) Photomicrograph of the fabricated device; (c) Block diagram of the testing system based on differential frequency processing; (d) Completed circuit board of the testing system.

2.2. Fabrication of Film Bulk Acoustic Resonator (FBAR) Device

The FBAR sensor was fabricated with a four-mask process using standard MEMS technology as shown in Figure 2a. First, a low-stress Si₃N₄ layer was grown on both sides of a (100) silicon wafer by low-pressure chemical vapor deposition. Then, an initial cavity was formed on one side of the wafer by wet etching (80 °C KOH) with the patterned Si₃N₄ layer as the mask. About 15-μm-thick silicon was left to support the following process on the other side of the wafer. Next, the Mo/AlN/Au piezoelectric stack was prepared by radio frequency magnetron sputtering and patterned by conventional photolithography technique. Finally, the residual silicon under the stack was etched by deep reactive ion etching to isolate the resonator acoustically from the substrate.

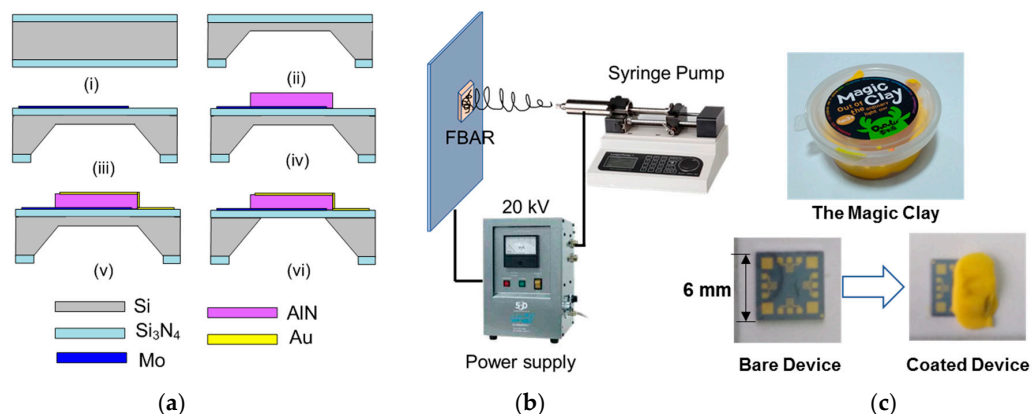


Figure 2. (a) Fabrication process of the FBAR formaldehyde sensor: (i) Growth of Si₃N₄ film; (ii) Etching of one side of the silicon wafer; (iii) Deposition and pattern of bottom Mo electrode; (iv) Deposition of AlN film; (v) Preparation of top Au electrode; (vi) Dry etching of the residual silicon. (b) Schematic diagram illustrating the electrospinning deposition of PEI nanofibers. (c) Photographs of the FBAR devices before and after the coating of clay.

2.3. Electrospinning Deposition of Polyethyleneimine (PEI) Nanofibers

After the fabrication process, the silicon wafer was cut into small pieces with the area of $6\text{ mm} \times 6\text{ mm}$ (as shown in Figure 2c). Two FBAR devices on the opposite side were used in this experiment as the detector and reference device, respectively. The reference device without sensitive layer was manually coated with kid's magic clay (DoDoLu, Zhigao colored clay Co., Ltd., Jinhua, China) before the electrospinning process (see Figure 2c). The main components of magic clay are polyethylene ethanol, cross-linking agent and water. The viscous magic clay was attached to the device surface and then was easily removed after natural drying without any damage on the device structure. The PEI aqueous solution (10 wt %, MW = 25,000, Macklin Biochemical Co., Ltd., Shanghai, China) was used as the electrospinning solution. The feed rate of the solutions was regulated at 5 mL/h by a syringe pump (LSP02, Longer Precision Pump Co., Ltd., Baoding, China). By applying the voltage of 20 kV between the syringe and the conductive sheet at a tip-to-collector distance of 20 cm, the nanofibers were continuously deposited on the FBAR device surface. After electrospinning, the device was dried at $40\text{ }^\circ\text{C}$ in vacuum for 30 min to evaporate the solvent. In addition, a flat PEI film was spin-coated (30 wt % PEI solution, 2500 rpm for 45 s) on the surface of another FBAR device to compare the formaldehyde sensing characteristics.

3. Results and Discussion

3.1. Characterization of the Resonator

The surface morphology of the sensitive coating on the FBAR surface was observed by a field emission scanning electron microscope (FE-SEM, S-4800 Hitachi, Tokyo, Japan) as shown in Figure 3. The average diameter of the PEI fibers was about 40 nm with random orientations. The distribution became denser with the increase of deposition time, which had an obvious effect on the formaldehyde response. Compared with the layer imbedded with nanoparticles [39] or nanotube [40] prepared by spin coating, the electrospinning method forms the three-dimensional structure, which can provide a larger specific surface area for vapor adsorption and diffusion.

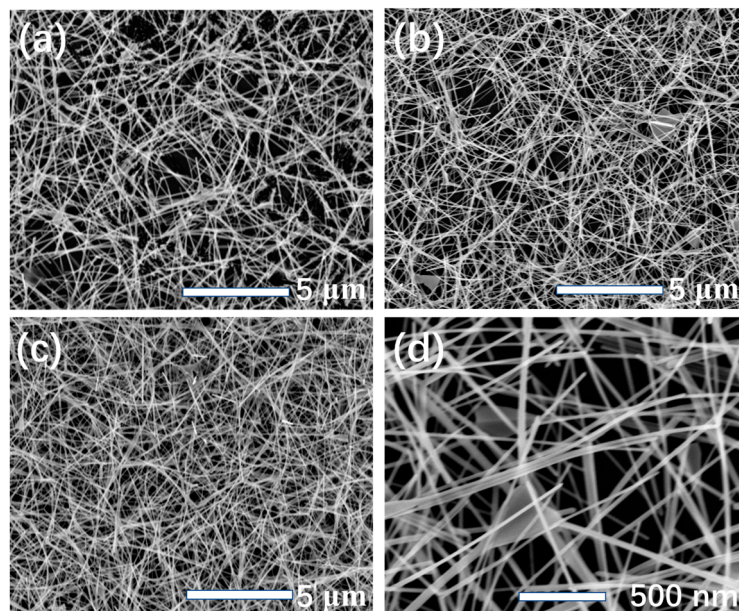


Figure 3. Typical FE-SEM images of the PEI nanofibers on the FBAR surface for the deposition times of (a) 50 s, (b) 150 s and (c) 300 s. The detail view of the nanofibers is shown in (d).

The thickness of the PEI nanofiber layers was estimated by the cross-view SEM images as shown in Figure 4. The thickness of the PEI nanofiber layer exhibited a linearly dependence on the deposition time with the rate of 3.185 nm/s. Figure 5 shows the admittance of the FBAR sensors coating with different amounts of nanofibers. The device frequency linearly went down from 4464.15 MHz to 4402.41 MHz with increasing nanofibers (Figure 6a). In addition, the Q factors of the FBAR devices were determined by the Butterworth–Van Dyke model [42] to evaluate the energy loss because of the sensitive coating. As shown in Figure 6b, the coated PEI nanofibers only caused a small influence on Q factors (<5%) when the deposition time was less than 150 s. However, the loading of superfluous fibers resulted in a dramatic degradation of Q factors, which may be ascribed to the scattering and absorption of acoustic energy from the porous structure on the wave propagation path. Besides, the resonant frequency of the bare device shows a temperature coefficient of frequency (TCF) of $-52.2 \text{ ppm}/^\circ\text{C}$ [43], which can be attributed to the thermal expansion of the piezoelectric film and the change of the acoustic velocity.

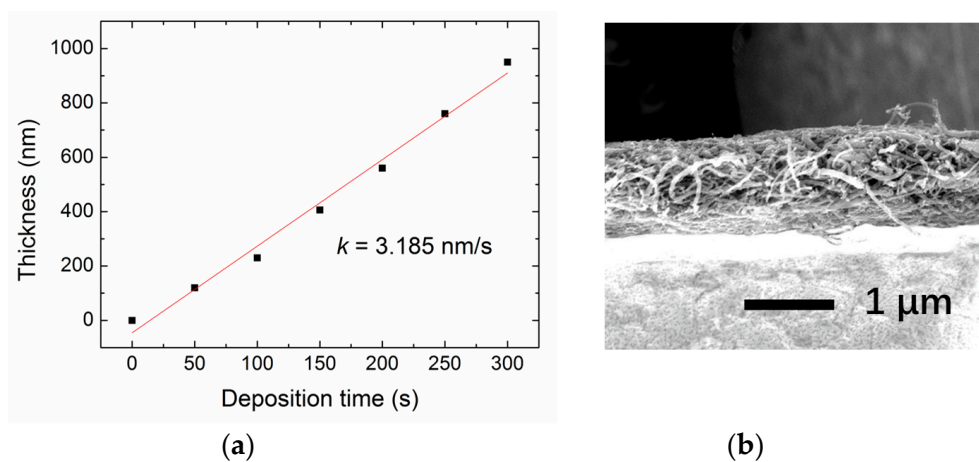


Figure 4. (a) Dependence of the thickness of the PEI nanofiber layer on the deposition time; (b) Typical cross-view SEM image of the PEI nanofiber layer with the deposition times of 300 s.

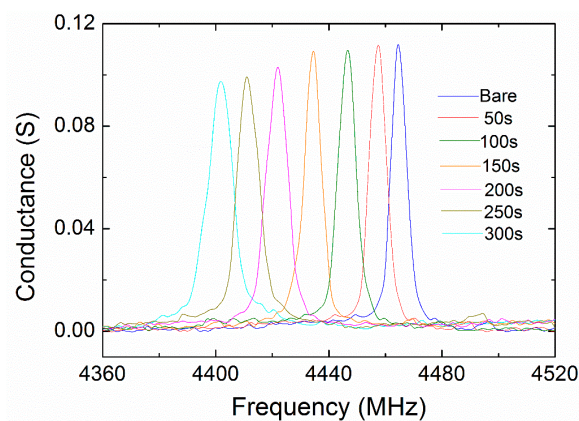


Figure 5. The admittance curves of the bare FBAR device and PEI nanofibers-coated FBAR devices. The times of electrospinning deposition were 50–300 s.

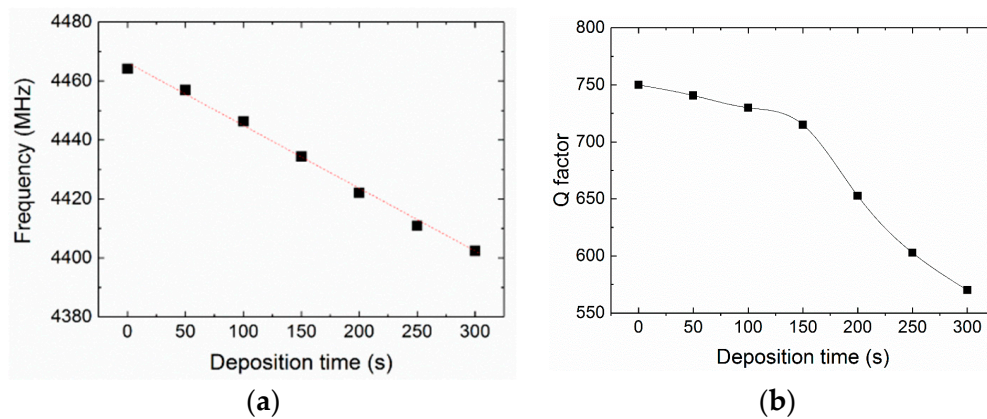


Figure 6. The changes of (a) resonant frequency and (b) Q factor of the PEI nanofibers-coated FBAR devices for different deposition times.

3.2. Effect of Deposition Time on the Formaldehyde Response

In the gas-sensing tests, the formaldehyde samples with required concentration were obtained by multiple dilution of the standard vapor (Changyuan Gas, Nanjing, China). All the gas tests were performed at the constant temperature condition (22 °C). Figure 7 shows the time-dependent frequency response of the FBAR sensors coated with flat PEI film and different amounts of PEI nanofibers in the formaldehyde vapor with the concentration of 300 ppb. Every sensing cycle comprised both absorption and desorption processes. At first, nitrogen was delivered to the test chamber and the stable resonant frequency was recorded as the baseline. After the formaldehyde was injected, the formaldehyde molecules were absorbed on the sensitive coating resulting in the downshift of resonant frequency. When the nitrogen was introduced again, the formaldehyde molecules were blown off from the sensitive coating and thus the response gradually raised to the baseline.

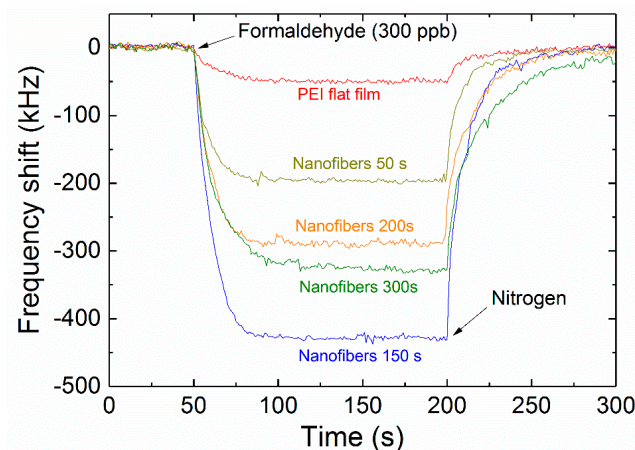


Figure 7. Time-dependent frequency response of the FBAR sensors coated with PEI flat film and different amounts of PEI nanofibers when exposed to 300 ppb formaldehyde vapor. All the tests were performed at room temperature and 40% relative humidity.

The structure and amount of the sensitive coating had an obvious influence on the absorption/desorption behavior of formaldehyde. At the formaldehyde concentration of 300 ppb, the response of the flat film coated sensor was very small (~50 kHz). As expected, the fibrous structure could absorb more molecules and significantly enhance the sensitivity. The adsorption of formaldehyde onto the sensitive coating is maintained by the polymeric amines in PEI via the reversible nucleophilic addition reaction to form Schiff base [38]. As shown in the SEM images, the PEI fibers were connected to each

other, forming net-like scaffolds, which increased the surface area and absorption sites and allowed the formaldehyde molecules to diffuse more easily inside the large space to react with the amine groups of PEI.

In particular, the sensor with the appropriate deposition time (150 s) exhibits the highest frequency downshift (~430 kHz) among the devices. Some references considered the coupled resonance between the microstructure coating and acoustic wave sensor [44–47]. However, in our study, the frequency shows a linearly negative shift with increasing of deposition time. The “drop and jump” change (the hallmark feature of coupled resonance) was not observed in Figure 6. On the other hand, the theoretical model proposed by Mansfeld [48] indicates that the mass-loading sensitivity increases sharply when the thickness of sensitive layer is close to a quarter of the acoustic wavelength. The Young modulus and acoustic velocity of solid-state PEI is 3.1–3.7 GPa and 2100–2300 m/s, respectively [49]. For the FBAR working frequency at 4.4 GHz, the corresponding quarter of the acoustic wavelength is 470–520 nm, which is very close to the thickness at the deposition time of 150 s in consideration of the velocity deviation between the solid state and nanofibers.

3.3. Sensitive Performance of the Optimized Sensor

On the basis of the above results, the optimized deposition time of 150 s was selected for further tests. Figure 8a shows the dynamic measurement of the optimized FBAR sensor exposed to the formaldehyde pulses with increasing concentrations. The fast adsorption and complete desorption took place with the response time of 10–25 s and the recovery time within 60 s. A saturated response was observed at vapor concentrations higher than 600 ppb, which is associated with the saturable adsorption of the PEI nanofibers. However, this detectable range could be accepted for the indoor air monitoring because serious throat and nasal irritation will occur when the formaldehyde concentration reaches about 1 ppm. As shown in Figure 8b, the frequency downshift of FBAR sensor was linearly proportional to the formaldehyde concentration before saturation with the regression coefficient (R^2) of 0.9921. The gas sensitivity, defined as the slope of calibration curve, was estimated to be -1.257 kHz/ppb over the linear region. The limit of detection (LOD) is given by $LOD = 3\sigma/S$, where S is the gas sensitivity of the sensor and σ is the average noise of the intrinsic frequency [50], respectively. Benefiting from the high mass-sensitivity and the porous structure of PEI fibrous coating, the LOD of the FBAR sensor was as low as 37 ppb ($\sigma \approx 15$ kHz). In comparison, the formaldehyde detection limit of a recently reported QCM sensor is 600 ppb [40]. The sensor noise determines the minimum detectable frequency shift and thus is related to the detection limit. In this study, the average noise level was about 15 kHz at the resonant frequency of 4.4 GHz, which is higher than that of commercialized QCM systems (typically 0.01 Hz/8 MHz). Even so, the FBAR sensor still exhibits a very high sensitivity and low detection limit. It is believed that the sensitivity can be further improved by optimizing the device structure and test circuit.

For the mass-loading sensors, the higher working frequency produces a larger frequency shift with the same mass change. Therefore, the FBAR sensor exhibits a gas sensitivity that was about ten times higher than that of the QCM formaldehyde sensors [37–39]. The LOD of FBAR sensor reached the same levels of MOS [3–5] and CNTs sensors [6–8]. Remarkably, in our case, we are able to employ the operation at room temperature and the integration capability into micro-electromechanical systems. Furthermore, compared with the analog resistance or current signals produced by MOS and CNTs sensors, the digitized frequency response used by FBAR is more robust and can be read out directly without the need of analog–digital conversion. Benefiting from the micrometer-scale size and the MEMS fabrication, an e-nose could be constructed by integrating a large number of FBAR devices with different sensitive coatings. Each sensor is sensitive to some analytes with different responses; thus, a fingerprint pattern is generated for specific target recognition from the complex environment. For example, Yao et al. [34] demonstrated an e-nose type gas sensor for the selective detection of volatile organic compounds based on the FBAR sensor array functionalized with four supramolecular monolayers (p-tert-butyl calix[8]-arene, porphine, β -cyclodextrin, and cucurbit[8]uril.).

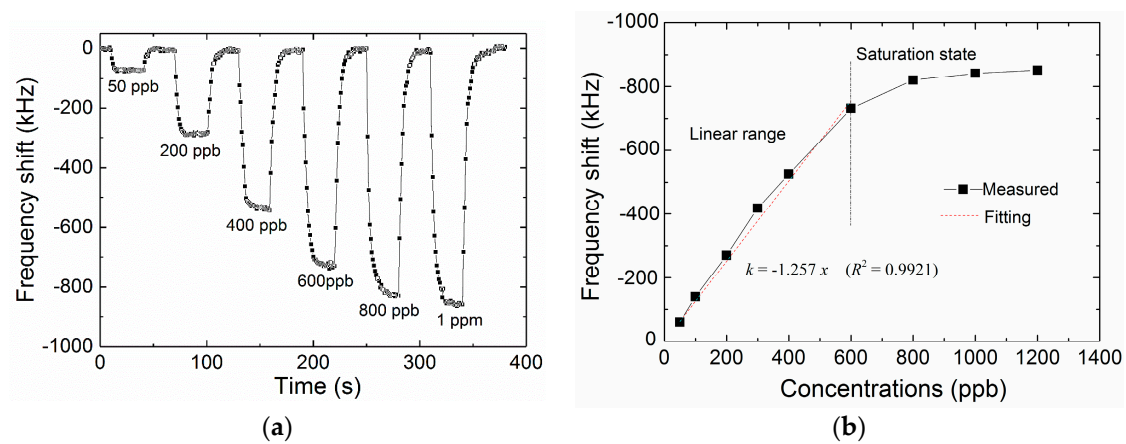


Figure 8. (a) Dynamic measurement of the FBAR sensor coated with PEI nanofibers exposed to the formaldehyde pulses with increasing concentrations at room temperature and 40% relative humidity; (b) Dependence of the frequency shift on the formaldehyde concentration.

3.4. Influence of Relative Humidity

In order to evaluate the influence of humidity on the sensing characteristics, the formaldehyde vapor mixed with saturated water vapor was delivered to the test chamber. Figure 9a shows the frequency response of the optimized FBAR sensor in three typical vapor concentrations measured at different ambient humidity. Both the frequency shift and the gas sensitivity were obviously enhanced with the increase of humidity. A possible reason is that the formaldehyde molecules could easily attach to the water molecules via hydrogen bonds [51]. In the humid environment, more water molecules were attached on the hydrophilic amine groups of PEI, and thus the adsorption capacity of the sensitive coating was improved.

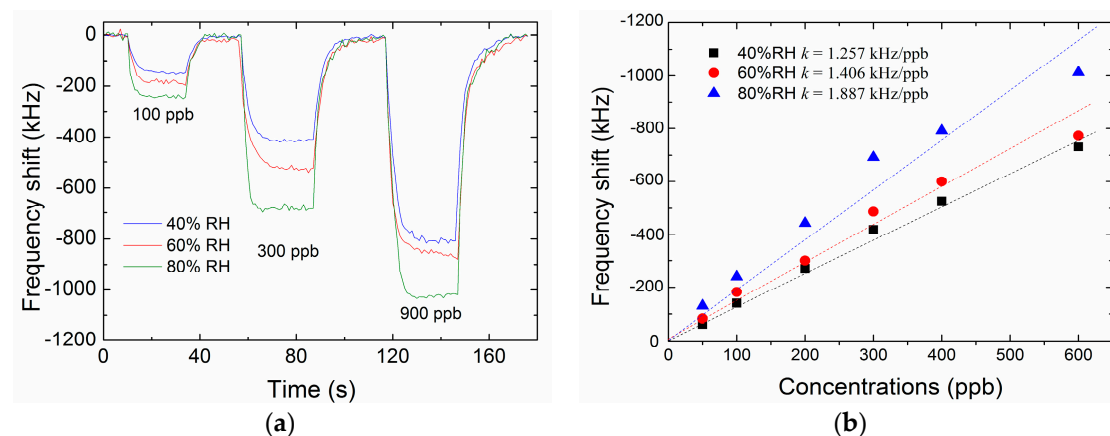


Figure 9. (a) Real-time frequency response of the optimized FBAR sensor exposed to three typical formaldehyde concentrations at the relative humidity of 40%, 60% and 80%. (b) Plots of frequency shift as a function of formaldehyde concentration at the relative humidity of 40%, 60% and 80%.

3.5. Selectivity of the Sensors

The FBAR sensor was tested against several potential indoor pollution vapors, including ethanol, acetone, benzene, dichloromethane, toluene and chloroform. As shown in Figure 10, the response to formaldehyde was about ten times higher than that of ethanol (the second largest response) indicating the excellent selectivity of the FBAR sensor coated with PEI nanofibers. As discussed before in Section 2.1, the main absorbing mechanism to formaldehyde is the nucleophilic addition

reaction between the carbon atoms in π -bonds (electrophile) and the nitrogen atoms in amine groups (nucleophile). As a result, the specific attachment to formaldehyde is significantly stronger than the physical or nonspecific adsorption of the interference vapors. Similar results were also observed in other PEI-based sensors [36–39].

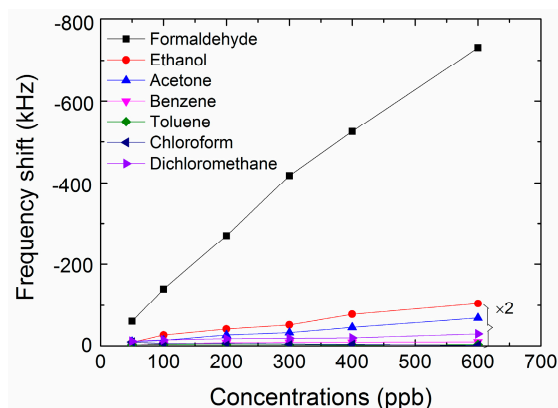


Figure 10. Plots of the frequency shift as a function of different concentration for formaldehyde and potential indoor pollution vapors.

4. Conclusions

In summary, we deposited PEI nanofibers on the FBAR mass-loading sensor by electrospinning and demonstrated its application for the detection of trace formaldehyde at room temperature. The interconnected PEI fibers formed a porous three-dimensional structure and provided a larger specific surface area to absorb formaldehyde molecules. The FBAR sensor exhibits a linear frequency downshift with increasing vapor concentration and excellent selectivity to formaldehyde with respect to other conventional organic vapors. The gas sensitivity is 1.216 kHz/ppb with the LOD of 37 ppb. The proposed FBAR device is a promising candidate as a mass-sensitive platform, and the studies of the electrospinning would benefit the developing of new sensitive coating for FBAR gas sensors.

Supplementary Materials: The following are available online at www.mdpi.com/2072-666X/9/2/62/s1, Figure S1: Details of the circuit design of the film bulk acoustic resonator (FBAR) testing system.

Acknowledgments: This work was supported by the National Science Foundations of China (Grant No. 61574086, 11504207), National Science Foundation of Shandong Province (Grant No. ZR2014AQ006), Qingdao science and technology program of basic research projects (Grant No. 15-9-1-78-jch), Project of Shandong Province Higher Educational Science and Technology Program (Grant No. J15LN17) and the Tai'shan Scholar Engineering Construction Fund of Shandong Province of China.

Author Contributions: Da Chen proposed the main idea and designed the device structure. Lei Yang and Hongfei Wang fabricated the device and prepared the nanofibers. Wenhua Yu, Maozeng Wu and Wei Wang tested the resonant characterization and performed the gas-sensing experiments. Lei Yang and Da Chen wrote the paper.

Conflicts of Interest: The authors declare no conflict of interest.

References

1. Davis, M.E.; Blicharz, A.P.; Hart, J.E.; Laden, F.; Garshick, E.; Smith, T.J. Occupational exposure to volatile organic compounds and aldehydes in the U.S. trucking industry. *Environ. Sci. Technol.* **2007**, *41*, 7152–7158. [[CrossRef](#)] [[PubMed](#)]
2. Marć, M.; Zabiegała, B.; Namieśnik, J. Testing and sampling devices for monitoring volatile and semi-volatile organic compounds in indoor air. *TrAC Trends in Anal. Chem.* **2012**, *32*, 76–86. [[CrossRef](#)]
3. Park, H.J.; Kim, J.; Choi, N.J.; Song, H.; Lee, D.S. Nonstoichiometric Co-rich ZnCo₂O₄ hollow nanospheres for high performance formaldehyde detection at ppb levels. *ACS Appl. Mater. Interfaces* **2016**, *8*, 3233–3240. [[CrossRef](#)] [[PubMed](#)]

4. Hu, P.; Han, N.; Zhang, D.; Ho, J.C.; Chen, Y. Highly formaldehyde-sensitive, transition-metal doped ZnO nanorods prepared by plasma-enhanced chemical vapor deposition. *Sens. Actuators B* **2012**, *169*, 74–80. [[CrossRef](#)]
5. Zheng, Y.; Wang, J.; Yao, P. Formaldehyde sensing properties of electrospun NiO-doped SnO₂ nanofibers. *Sens. Actuators B* **2011**, *156*, 723–730. [[CrossRef](#)]
6. Yoosefian, M.; Raissi, H.; Mola, A. The hybrid of Pd and SWCNT (Pd loaded on SWCNT) as an efficient sensor for the formaldehyde molecule detection: A DFT study. *Sens. Actuators B* **2015**, *212*, 55–62. [[CrossRef](#)]
7. Mu, H.; Wang, K.; Zhang, S.; Shi, K.; Sun, S.; Li, Z.; Zhou, J.; Xie, H. Fabrication and characterization of amino group functionalized multiwall carbon nanotubes (MWCNT) formaldehyde gas sensors. *IEEE Sens. J.* **2014**, *14*, 2362–2368. [[CrossRef](#)]
8. Xie, H.; Sheng, C.; Chen, X.; Wang, X.; Li, Z.; Zhou, J. Multi-wall carbon nanotube gas sensors modified with amino-group to detect low concentration of formaldehyde. *Sens. Actuators B* **2012**, *168*, 34–38. [[CrossRef](#)]
9. Antwi-Boampong, S.; Peng, J.S.; Carlan, J.; Belbruno, J.J. A molecularly imprinted fluoral-p/polyaniline double layer sensor system for selective sensing of formaldehyde. *IEEE Sens. J.* **2014**, *14*, 1490–1498. [[CrossRef](#)]
10. Ruppel, C.C.W. Acoustic wave filter technology—A review. *IEEE Trans. Ultrason. Ferroelectr. Freq. Control* **2017**, *64*, 1390–1400. [[CrossRef](#)] [[PubMed](#)]
11. Hashimoto, K.Y. Radio frequency bulk acoustic wave filters: Current status and future prospective. *IEEE Trans. Electron. Inf. Syst.* **2013**, *133*, 502–508. [[CrossRef](#)]
12. Zhu, Y.; Wang, N.; Sun, C.; Merugu, S.; Singh, N.; Gu, Y. A High Coupling Coefficient 2.3-GHz AlN Resonator for High Band LTE Filtering Application. *IEEE Electron Device Lett.* **2016**, *37*, 1344–1346. [[CrossRef](#)]
13. Wang, J.; Chen, D.; Gan, Y.; Sun, X.; Jin, Y. High sensitive self-assembled monolayer modified solid mounted resonator for organophosphate vapor detection. *Appl. Surf. Sci.* **2011**, *257*, 4365–4369. [[CrossRef](#)]
14. Zhao, X.; Ashley, G.M.; Garcia-Gancedo, L.; Jin, H.; Luo, J.; Flewitt, A.J.; Lu, J.R. Protein functionalized ZnO thin film bulk acoustic resonator as an odorant biosensor. *Sens. Actuators B* **2012**, *163*, 242–246. [[CrossRef](#)]
15. Chen, D.; Wang, J.J.; Li, D.H.; Xu, Y. Hydrogen sensor based on Pd-functionalized film bulk acoustic resonator. *Sens. Actuators B* **2011**, *159*, 234–237. [[CrossRef](#)]
16. Chang, Y.; Tang, N.; Qu, H.; Liu, J.; Zhang, D.; Zhang, H.; Pang, W.; Duan, X. Detection of volatile organic compounds by self-assembled monolayer coated sSensor array with concentration-independent fingerprints. *Sci. Rep.* **2016**, *6*. [[CrossRef](#)]
17. Zhao, X.; Pan, F.; Ashley, G.M.; Garcia-Gancedo, L.; Luo, J.; Flewitt, A.J.; Milne, W.I.; Lu, J.R. Label-free detection of human prostate-specific antigen (HPSA) using film bulk acoustic resonators (FBARs). *Sens. Actuators B* **2014**, *190*, 946–953. [[CrossRef](#)]
18. Chen, D.; Wang, J.; Wang, P.; Guo, Q.; Zhang, Z.; Ma, J. Real-time monitoring of human blood clotting using a lateral excited film bulk acoustic resonator. *J. Micromech. Microeng.* **2017**, *27*, 045013. [[CrossRef](#)]
19. Voiculescu, I.; Nordin, A.N. Acoustic wave based MEMS devices for biosensing applications. *Biosens. Bioelectron.* **2012**, *33*, 1–9. [[CrossRef](#)] [[PubMed](#)]
20. Chen, D.; Song, S.; Ma, J.; Zhang, Z.; Wang, P.; Liu, W.; Guo, Q. Micro-electromechanical film bulk acoustic sensor for plasma and whole blood coagulation monitoring. *Biosens. Bioelectron.* **2017**, *91*, 465–471. [[CrossRef](#)] [[PubMed](#)]
21. Pang, W.; Zhao, H.; Kim, E.S.; Zhang, H.; Yuc, H.; Hu, X. Piezoelectric microelectromechanical resonant sensors for chemical and biological detection. *Lab Chip* **2012**, *12*, 29–44. [[CrossRef](#)] [[PubMed](#)]
22. Chen, D.; Wang, J.; Xu, Y.; Li, D. A pure shear mode ZnO film resonator for the detection of organophosphorous pesticides. *Sens. Actuators B* **2012**, *171–172*, 1081–1086. [[CrossRef](#)]
23. Chen, D.; Zhang, Z.; Ma, J.; Wang, W. ZnO Film Bulk Acoustic Resonator for the Kinetics Study of Human Blood Coagulation. *Sensors* **2017**, *17*, 1015. [[CrossRef](#)] [[PubMed](#)]
24. Chen, D.; Wang, J.; Li, D.; Liu, Y.; Song, H.; Liu, Q. A poly(vinylidene fluoride)-coated ZnO film bulk acoustic resonator for nerve gas detection. *J. Micromech. Microeng.* **2011**, *21*, 085017–085023. [[CrossRef](#)]
25. Wang, J.-J.; Liu, W.-H.; Chen, D.; Xu, Y.; Zhang, L.-Y. A micro-machined thin film electro-acoustic biosensor for detection of pesticide residuals. *J. Zhejiang Univ.-Sci. C-Comput. Electron.* **2014**, *15*, 383–389. [[CrossRef](#)]
26. Zhang, M.; Huang, J.; Cui, W.; Pang, W.; Zhang, H.; Zhang, D.; Duan, X. Kinetic studies of microfabricated biosensors using local adsorption strategy. *Biosens. Bioelectron.* **2015**, *74*, 8–15. [[CrossRef](#)] [[PubMed](#)]
27. Wang, J.; Chen, D.; Xu, Y.; Liu, W. Label-free immunosensor based on micromachined bulk acoustic resonator for the detection of trace pesticide residues. *Sens. Actuators B* **2014**, *190*, 378–383. [[CrossRef](#)]

28. Guo, P.; Xiong, J.; Zheng, D.; Zhang, W.; Liu, L.; Wang, S.; Gu, H. A biosensor based on a film bulk acoustic resonator and biotin-avidin system for the detection of the epithelial tumor marker mucin 1. *RSC Adv.* **2015**, *5*, 66355–66359. [[CrossRef](#)]
29. Campos, J.; Jiménez, C.; Trigo, C.; Ibarra, P.; Rana, D.; Thiruganesh, R.; Ramalingam, M.; Haidar, Z.S. Quartz crystal microbalance with dissipation monitoring: A powerful tool for bionanoscience and drug discovery. *J. Bionanosci.* **2015**, *9*, 249–260. [[CrossRef](#)]
30. Wu, Z.; Chen, X.; Zhu, S.; Zhou, Z.; Yao, Y.; Quan, W.; Liu, B. Enhanced sensitivity of ammonia sensor using graphene/polyaniline nanocomposite. *Sens. Actuators B* **2013**, *178*, 485–493. [[CrossRef](#)]
31. Khassaf, H.; Khakpash, N.; Sun, F.; Sbrockey, N.M.; Tompa, G.S.; Kalkur, T.S.; Alpay, S.P. Strain engineered barium strontium titanate for tunable thin film resonators. *Appl. Phys. Lett.* **2014**, *104*, 202902. [[CrossRef](#)]
32. Chen, D.; Wang, J.; Xu, Y.; Li, D.; Zhang, L.; Li, Z. Highly sensitive detection of organophosphorus pesticides by acetylcholinesterase-coated thin film bulk acoustic resonator mass-loading sensor. *Biosens. Bioelectron.* **2013**, *41*, 163–167. [[CrossRef](#)] [[PubMed](#)]
33. Chen, D.; Wang, J.; Xu, Y. Highly sensitive lateral field excited piezoelectric film acoustic enzyme biosensor. *IEEE Sens. J.* **2013**, *13*, 2217–2222. [[CrossRef](#)]
34. Lu, Y.; Chang, Y.; Tang, N.; Qu, H.; Liu, J.; Pang, W.; Zhang, H.; Zhang, D.; Duan, X. Detection of volatile organic compounds using microfabricated resonator array functionalized with supramolecular monolayers. *ACS Appl. Mater. Interfaces* **2015**, *7*, 17893–17903. [[CrossRef](#)] [[PubMed](#)]
35. Chen, D.; Wang, J.; Li, D.; Xu, Y.; Li, Z. Solidly mounted resonators operated in thickness shear mode based on c-axis oriented AlN films. *Sens. Actuators A* **2011**, *165*, 379–384. [[CrossRef](#)]
36. Jingjing, W.; Da, Z.; Ke, W.; Weiwei, H. The detection of formaldehyde using microelectromechanical acoustic resonator with multiwalled carbon nanotubes-polyethyleneimine composite coating. *J. Micromech. Microeng.* **2018**, *28*, 015003.
37. Zhang, C.; Wang, X.; Lin, J.; Ding, B.; Yu, J.; Pan, N. Nanoporous polystyrene fibers functionalized by polyethyleneimine for enhanced formaldehyde sensing. *Sens. Actuators B* **2011**, *152*, 316–323. [[CrossRef](#)]
38. Wang, X.; Ding, B.; Sun, M.; Yu, J.; Sun, G. Nanofibrous polyethyleneimine membranes as sensitive coatings for quartz crystal microbalance-based formaldehyde sensors. *Sens. Actuators B* **2010**, *144*, 11–17. [[CrossRef](#)]
39. Wang, X.; Cui, F.; Lin, J.; Ding, B.; Yu, J.; Al-Deyab, S.S. Functionalized nanoporous TiO₂ fibers on quartz crystal microbalance platform for formaldehyde sensor. *Sens. Actuators B* **2012**, *171–172*, 658–665. [[CrossRef](#)]
40. Tai, H.; Bao, X.; He, Y.; Du, X.; Xie, G.; Jiang, Y. Enhanced formaldehyde-sensing performances of mixed polyethyleneimine-multiwalled carbon nanotubes composite films on quartz crystal microbalance. *IEEE Sens. J.* **2015**, *15*, 6904–6911. [[CrossRef](#)]
41. Li, L.; Xiang, Y.; Shang, Y. *Basic Organic Chemistry*; Tsinghua University Press: Beijing, China, 2008; pp. 350–351. ISBN 9787302186571.
42. Zhang, H.; Marma, M.S.; Kim, E.S.; McKenna, C.E. Thompson, M.E. A film bulk acoustic resonator in liquid environments. *J. Micromech. Microeng.* **2005**, *15*, 1911–1916. [[CrossRef](#)]
43. Chen, D.; Song, S.; Zhang, D.; Wang, P.; Liu, W. Sensing characteristics of pure-shear film bulk acoustic resonator in viscous liquids. *Mod. Phys. Lett. B* **2017**, *31*, 1750086. [[CrossRef](#)]
44. Wang, P.; Su, J.; Dai, W.; Cernigliaro, G.; Sun, H. Ultrasensitive quartz crystal microbalance enabled by micropillar structure. *Appl. Phys. Lett.* **2014**, *104*, 043504. [[CrossRef](#)]
45. Wang, P.; Su, J.; Su, C.F.; Dai, W.; Cernigliaro, G.; Sun, H. An ultrasensitive quartz crystal microbalance-micropillars based sensor for humidity detection. *J. Appl. Phys.* **2014**, *115*, 224501. [[CrossRef](#)]
46. Chung, P.R.; Tzeng, C.T.; Ke, M.T.; Lee, C.Y. Formaldehyde gas sensors: A review. *Sensors* **2013**, *13*, 4468–4484. [[CrossRef](#)] [[PubMed](#)]
47. Pramod, N.G.; Pandey, S.N.; Sahay, P.P. Sn-doped In₂O₃ nanocrystalline thin films deposited by spray pyrolysis: Microstructural, optical, electrical, and formaldehyde-sensing characteristics. *J. Therm. Spray Technol.* **2013**, *22*, 1035–1043. [[CrossRef](#)]
48. Mansfeld, G.D. Theory of high overtone bulk acoustic wave resonator as a gas sensor. In Proceedings of the 13th International Conference on Microwaves, Radar and Wireless Communications, MIKON 2000, Wroclaw, Poland, 22–24 May 2000; pp. 469–472.
49. Cranston, E.D.; Eita, M.; Johansson, E.; Netrval, J.; Salajková, M.; Arwin, H.; Wagberg, L. Determination of Young's modulus for nanofibrillated cellulose multilayer thin films using buckling mechanics. *Biomacromolecules* **2011**, *12*, 961–969. [[CrossRef](#)] [[PubMed](#)]

50. Penza, M.; Aversa, P.; Cassano, G.; Suriano, D.; Wlodarski, W.; Benetti, M.; Cannatà, D.; Pietrantonio, F.D.; Verona, E. Thin-film bulk-acoustic-resonator gas sensor functionalized with a nanocomposite langmuir-blodgett layer of carbon nanotubes. *IEEE Trans. Electron Devices* **2008**, *55*, 1237–1243. [[CrossRef](#)]
51. Dimitrova, Y. Solvent effects on vibrational spectra of hydrogen-bonded complexes of formaldehyde and water: An ab initio study. *J. Mol. Struct. THEOCHEM* **1997**, *391*, 251–257. [[CrossRef](#)]



© 2018 by the authors. Licensee MDPI, Basel, Switzerland. This article is an open access article distributed under the terms and conditions of the Creative Commons Attribution (CC BY) license (<http://creativecommons.org/licenses/by/4.0/>).